Comments on diffraction modelling

John C. Bancroft

ABSTRACT

Seismic data can be modelled by spreading energy along a diffraction shape. Energy spread along the diffraction should be a wavelet that is high cut filtered. However, single time samples are often used to reduce the computer runtime, but will introduce aliasing artifacts. Additional filtering techniques may be required to reduce these artifacts.

Diffraction modelling is used to illustrate the differences in the amplitudes of diffractions produced from a scatterpoint or from the termination of a reflector. This type of modelling introduces a phase shift to the data that require correction for accurate modelling. Aliasing artifacts may be produced, especially from horizontal reflectors. These problems are illustrated, discussed, and evaluated.

INTRODUCTION

Seismic data can be modelled by spreading energy on a seismic section. The input data would typically be a section defined with the reflectivity of the geological model. Diffraction energy is created for each sample and for all traces in the section. The input section may be in depth, and the diffraction shape computed from the velocity model. The input section may also be in time and the diffraction shape computed using a hyperbolic equation, using a velocity that is constant or of an RMS type.

I will assume that the model is defined in time, and will use a hyperbolic diffraction shape for time t defined by

$$t^2 = t_0^2 + \frac{4h^2}{v^2} \tag{1}$$

where t_0 is the vertical two way time, h is half the source receiver offset and v is a constant velocity or an RMS type velocity.

A goal of this modelling is to ensure there is no aliased energy present in the final modelled section. Aliasing may be prevented by choosing a wavelet that varies along the diffraction to attenuate high frequencies. This is an expensive process for computer run-times and is often ignored. The wavelet is typically replaced with a single time value, requiring the input data, or the output data, to be filtered with high cut filters or with specially designed FK filters.

The maximum frequency for filters that are used to prevent aliasing are computed with parameters from the geometry of the input and output data. The maximum frequency f_{max} is defined using the aliasing equation

$$f_{\max} = \frac{v}{4 \times \delta x \times \tan(\theta)} \tag{2}$$

where v is the velocity, δx the trace spacing, and θ the dip angle. The dip may be defined as part of the input data, or as the dip along the diffraction. After modelling, the maximum apparent dip on the modeled section will be 45 degrees, allowing the tangent term to be unity and dropped from the equation.

The maximum frequency can be controlled by bandpass filtering the input data, or by using a band-limited diffraction that may have a single bandwidth, or by using a diffraction in which the bandwidth varies with the offset h.

A band-limited diffraction will spread energy over a number of samples, (a wavelet), on each output trace and this may result in expensive for run times. Therefore, the input data would normally be band limited to allowing the spreading diffraction to be limited to one sample on each of the output traces. In this case, the diffraction is aliased and can lead to aliasing of the modelled data, if that data has not been band limited to the maximum frequency defined by the input geometry.

It is often assumed that horizontal events are not subject to aliasing as their dip is zero and the maximum frequency could be infinite as indicated by equation (2). That is not always the case as amplitudes along the event may vary, or the flat events may be truncated, spreading energy to dips beyond the assumed zero degrees. In addition, an aliased diffraction, such as those used in modelling and migration, can create aliased energy from the horizontal events.

I will illustrate the aliasing problem using modelling with diffractions from Lab1, used in my Modelling, Migration, and Inversion course.

DIFFRACTION MODELLING

Examining a single diffraction

Figure 1a contains a single diffraction at t_0 = 100 ms in a section that has a trace interval of 20 meters with a velocity v = 3,000 m/sec. The data is sampled at 2 ms or with a sampling frequency of 500 Hz, and a Nyquist frequency is 250 Hz. A t_0/t taper was applied where t_0 is the time of the input sample (or apex of the diffraction), and t is the time of the output sample on the diffraction.

The modelled section should be dip limited (as required) to a maximum dip of 45 degrees. The maximum frequency to prevent aliasing, according to equation (2), is 37.5 Hz. However, the diffraction contains very high frequencies as it was band-pass filtered using corner frequencies at 1, 5, 200, and 249 Hz, with low and high transition bands using a raised cosine shape. The wavelet from the filter is zero phase.

The amplitude of the FK transform of the diffraction is shown in Figure 1b. The 45 degree dip limit of the diffraction reaches the spatial frequency boundary at a frequency of 37.5 Hz, defined by the aliasing equation. The dipping energy continues to wrap around in the frequency domain as illustrated by the crisscrossing energy above 37.5 Hz. Parts (c) and (d) of this figure contain the same diffraction and FK transform, however the amplitude of the diffraction in (c) is increased, and the FK plot (d) contains a diamond shape area identifying unaliased data.

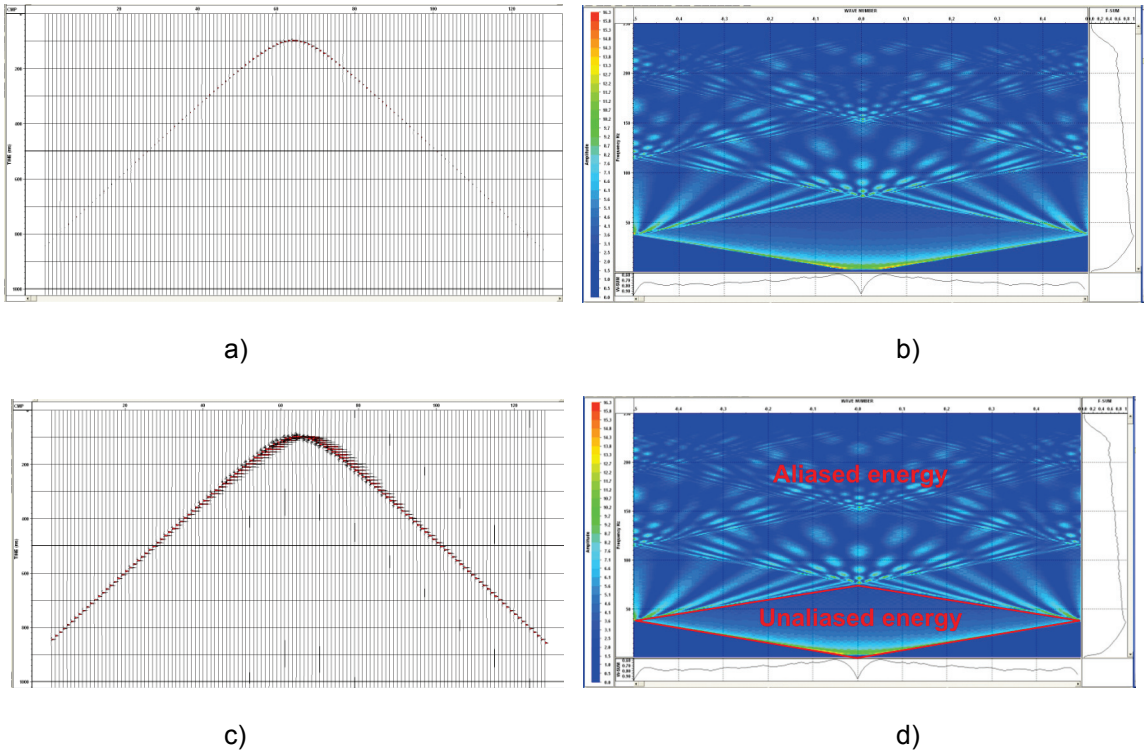

FIG. 1. A diffraction with bandpass filter (1,5,200,249), a) with peak amplitude at one trace interval, b) ten times the amplitude of (a), c) the amplitude spectrum with linear amplitudes illustrating the aliasing, and d) the same amplitude spectrum including a red trapezoid identifying energy that is not aliased.

Modelling in the time domain is essentially a convolution process of the diffraction with the input data, but in the frequency domain it is a product of the FK transforms of the diffraction and input data.

A rather "obvious" conclusion would be to band limit the diffraction to a much lower frequency as illustrated in Figures 2a and c. The diffraction was band pass filtered using a 1, 5, 32, and 38 Hz filter to limit the maximum frequency to that defined by the aliasing equation to be 37.5 Hz. The amplitudea of the FK spectra are shown with a linear (b) and db scale (d), with the db scale emphasizing the amplitude of the very low energy above the 45 degree dip limit caused by the truncation at the ends of the diffraction. If we assume that the amplitude of this FK display is zero above 37.5 Hz, then its multiplication with the input data will restrict it to the same 37.5 Hz. For example, it will limit zero dip energy to 37.5 degrees, even though a horizontal event should be able to contain much higher frequencies.

Note the aliased energy for zero dip in Figure 1 is above 75 Hz., where the wavenumber is k = 0. Other dips from zero to 45 degrees will be limited by a corresponding line to 37.5 Hz at the spatial Nyquist frequency. Consequently, at this point, the best filter would be an FK filter designed to attenuate energy above the red trapezoid in Figure 1d. All aliased energy will be attenuated, and a horizontal event will have a maximum frequency of 75 Hz.

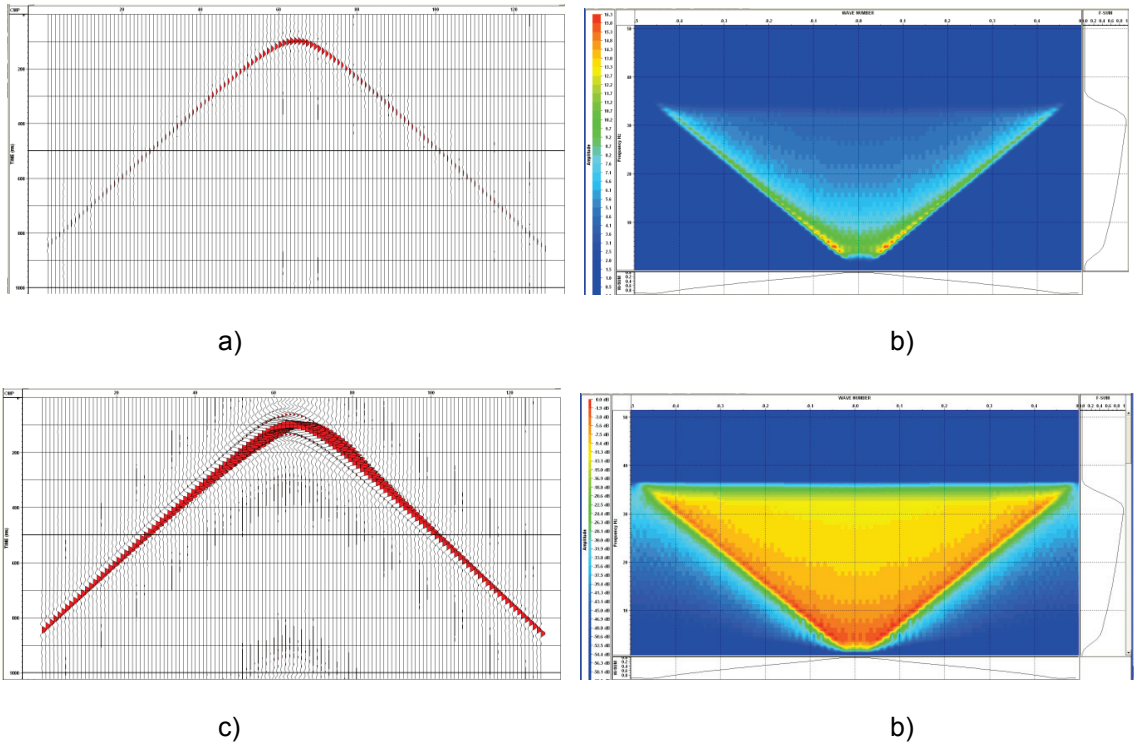

a) b)

c) b)

FIG. 2. A diffraction with bandpass filter (1,5,32,38) to prevent aliasing, a) with peak amplitude at one trace interval, d) the amplitude spectrum with linear amplitudes, c) ten times the amplitude of (a), and d) the amplitude spectrum displayed with a db scale.

Examining a short row of diffractions

Figure 3 shows a close-up of the diffraction modelling of ten horizontal samples with the high frequency filter. The modelling of a horizontal event should produce a horizontal event with diffractions at the ends, and a cancellation of the interior diffractions. That is not the case in Figure 3a, where we see the replication of the diffraction ten times with no apparent cancellation. In fact, we can see the beginning of horizontal events for each wavelet on the diffractions as evident in the FK plot in Figure 3b.

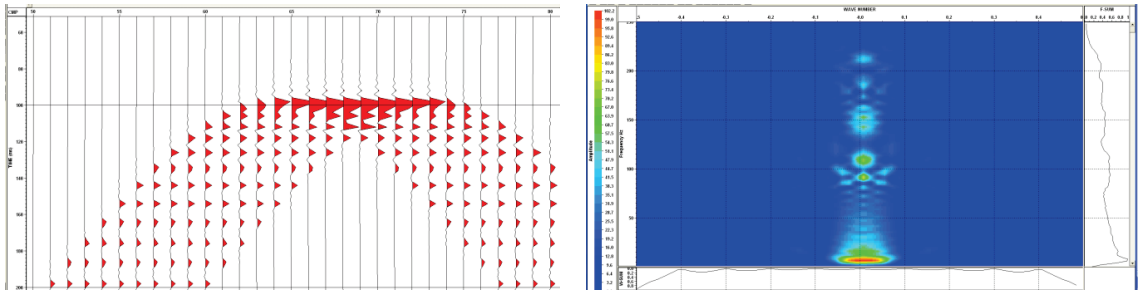

a) b)

FIG. 3. Diffraction modelling with a) ten input samples and b) the linear amplitude spectrum.

In the Fk plot of Figure 3b, the energy is tending to the central zero wavenumber for horizontal events, but there is still dispersed energy. This energy is more visible in Figure 4 that shows the amplitudes of Figure 3b with a db amplitude scale.

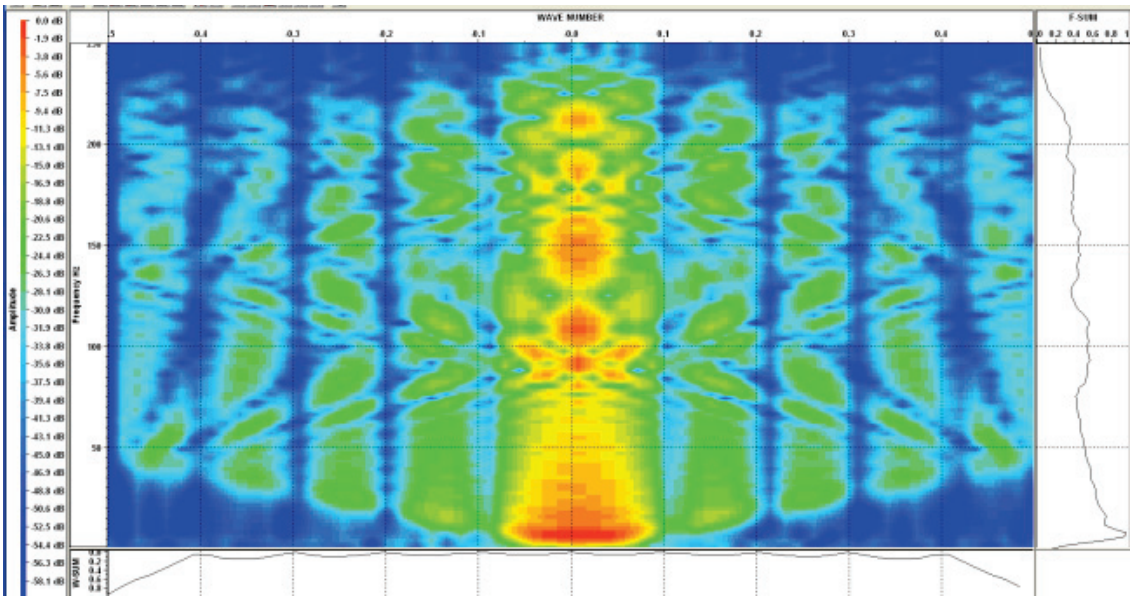

FIG. 4. FK amplitude spectrum of Figure 3, but with a db amplitude scale.

Near the apex of the diffractions in Figure 3a, the vertical, or time movement of the diffraction wavelet is small, and when repeated horizontally, tends to create horizontal events at very high frequencies. As we proceed down the section, horizontal event appear with an increased spacing or lower frequency.

These apparent horizontal events cluster around the central zero wavenumber in the FK plots.

A large row of high frequency reflectors

A large row of diffractions that are "modelled" on a high frequency linear reflection are displayed in Figure 5a, with the linear (b) and db amplitude (c) FK plots. Again we see the clustering of the multitude of horizontal reflections in (a) that cluster around the zero wavenumber. In the db FK plot (c), we see amplitudes similar to the example of the single high frequency diffraction.

At the steeper parts of the diffractions, the slope is tending to be constant at 45 degrees, and the spacing of the apparent horizontal reflectors tends also to be constant. When the trace spacing is 20 meters, the vertical spacing of a 45 degree slope will also be 20 meters but is expressed in two-way time as 3000/(2x20) = 75 Hz. We can see this as the large amplitude blob on the FK plots at the zero wavenumber and at 75 and 150 Hz.

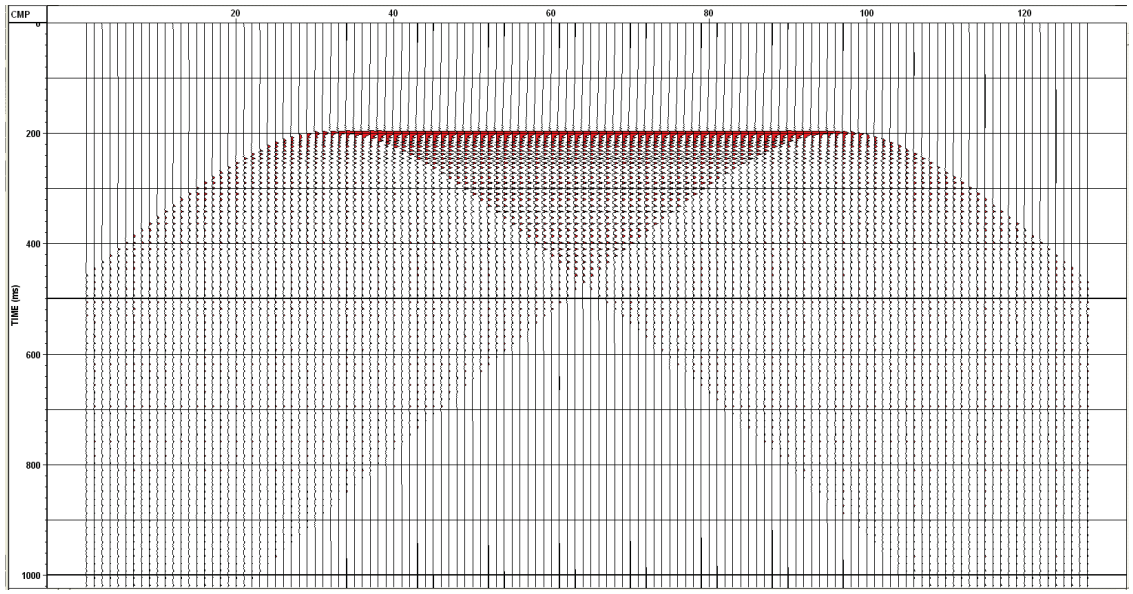

a) b)

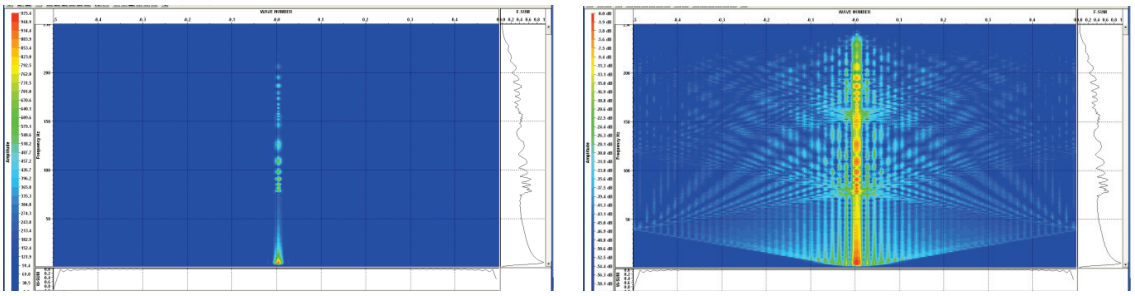

b) c)

FIG. 5. A large horizontal event with the high frequency wavelet in a) showing many horizontal events, with b) the linear amplitude and c) the db amplitude Fk plots.

We will now start to apply a bandpass filter with a lower high cut frequency as illustrated in Figures 6 to 9.

A 1, 5, 100, 150 Hz filter was applied to the data in Figure 6, and the blob of energy at 150 Hz is removed. This is barely evident as the removal of the high frequencies in the wavelets close to the desired reflection.

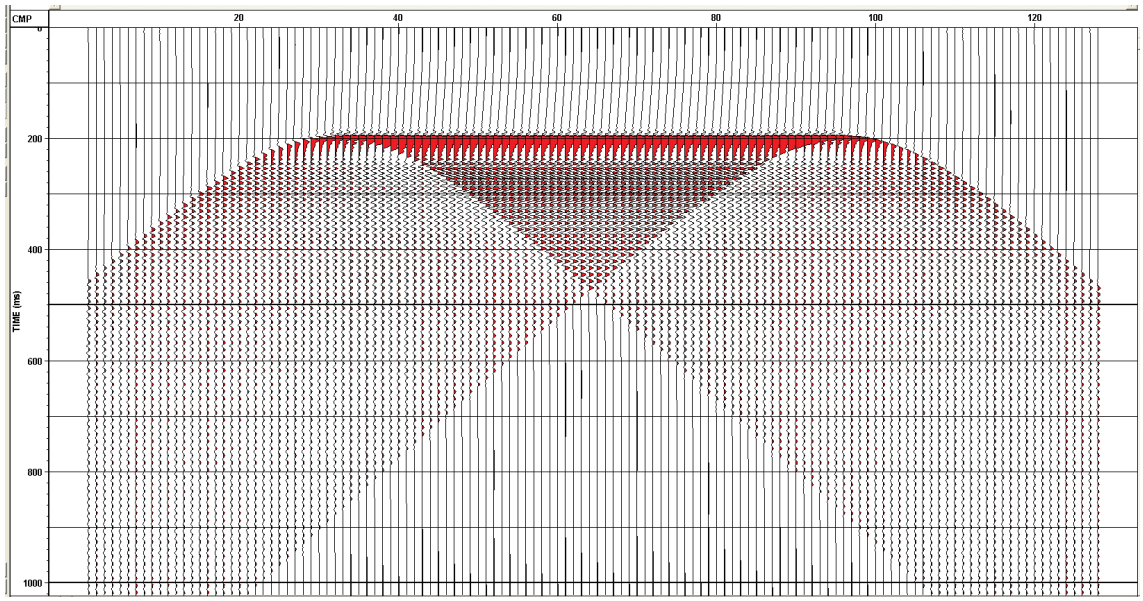

a)

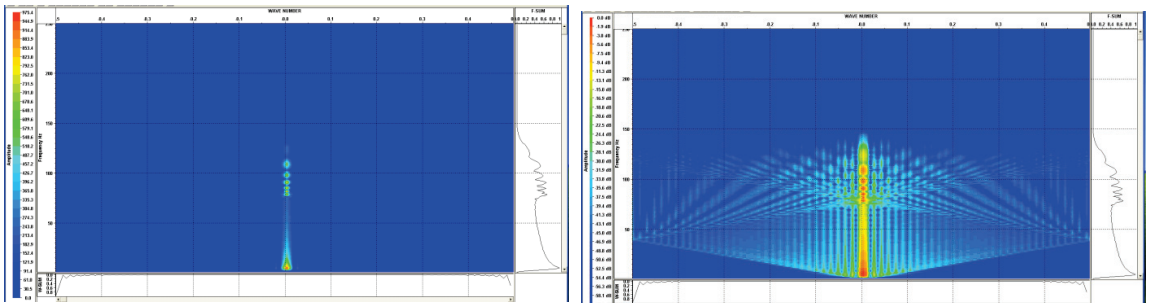

b) c)

FIG. 6. A large horizontal event with mid frequency wavelet (1,5,100,150) in a) showing many horizontal events, with b) the linear amplitude and c) the db amplitude FK plots.

In Figure 7, a filter 1, 5, 70 ,100 Hz was applied that removes the energy at 140 Hz. We can now see the attenuation of the horizontal events between 200 and 400 ms. The apparent horizontal events below 400 ms can be seen on the FK plot just above 75 Hz.

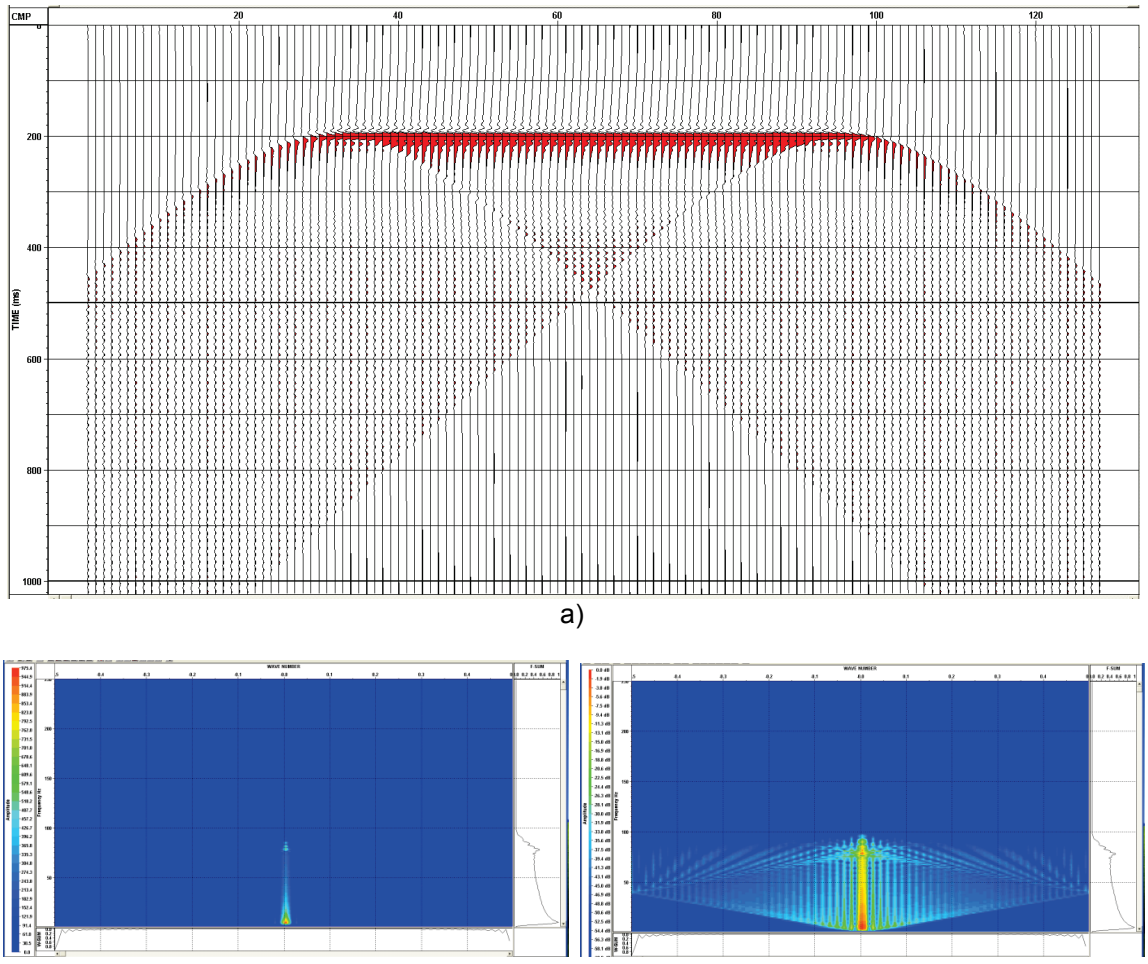

a)

b) c)

FIG. 7. A large horizontal event with mid frequency wavelet (1,5,70,100) in a) showing many horizontal events, with b) the linear amplitude and c) the db amplitude FK plots.

A high cut filter 1, 5, 70, 75 Hz attenuated the aliased energy at 75 Hz and appears to have removed all the aliased horizontal events. The energy aliased at $k = 0$ has now been remove with a very sharp high cut filter, i. e. from 70 to 75 Hz. This sharp cutoff causes excessive ringing in the wavelet of the flat event and the diffractions at the edge of the horizontal event. The low cut filter also has caused a large low frequency bias on the wavelet. These effects are reduced in the following example where the bandpass filter is 5, 15, 50, 75 Hz.

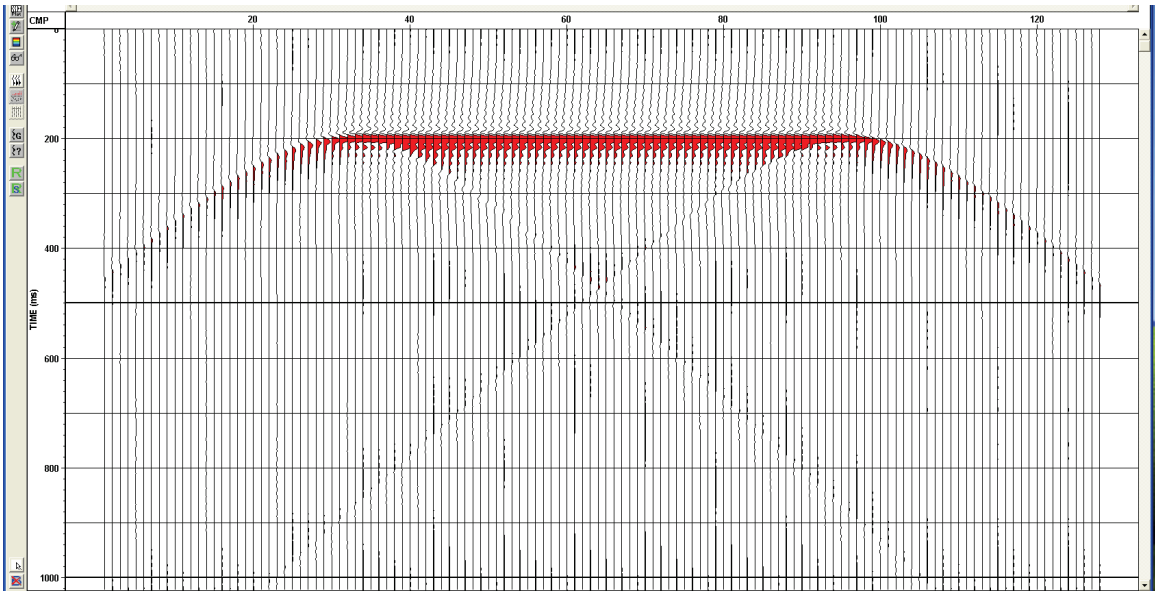

a)

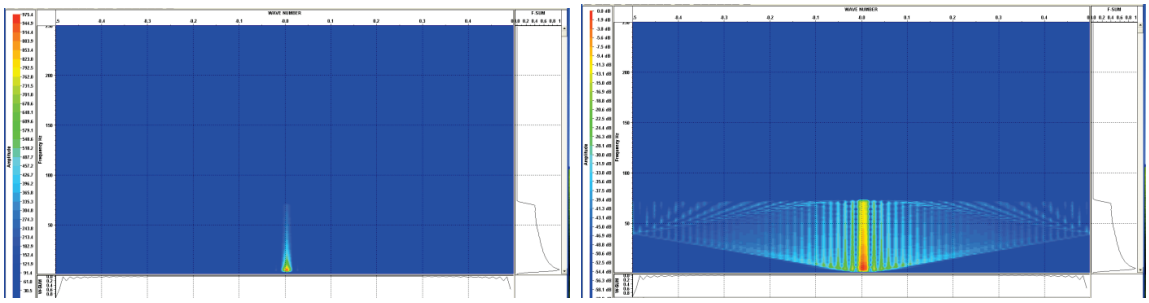

b) c)

FIG. 8. A large horizontal event with mid frequency wavelet (1,5,70,75) in a) showing many horizontal events, with b) the linear amplitude and c) the db amplitude FK plots.

The application of a filter 5, 15, 50, 75 Hz with more gradual tapers on the low and high ends is illustrated in Figure 9. We observe that the low frequencies of the wavelet are removed along with the excessive ringing of the wavelet. There will still be some aliased energy above the line from 75 Hz at k = 0, to 37.5 Hz at the Nyquist spatial frequency that is visible on Figure 8c, but is negligible in Figure 9. Dipping events may have some aliased energy with this filter.

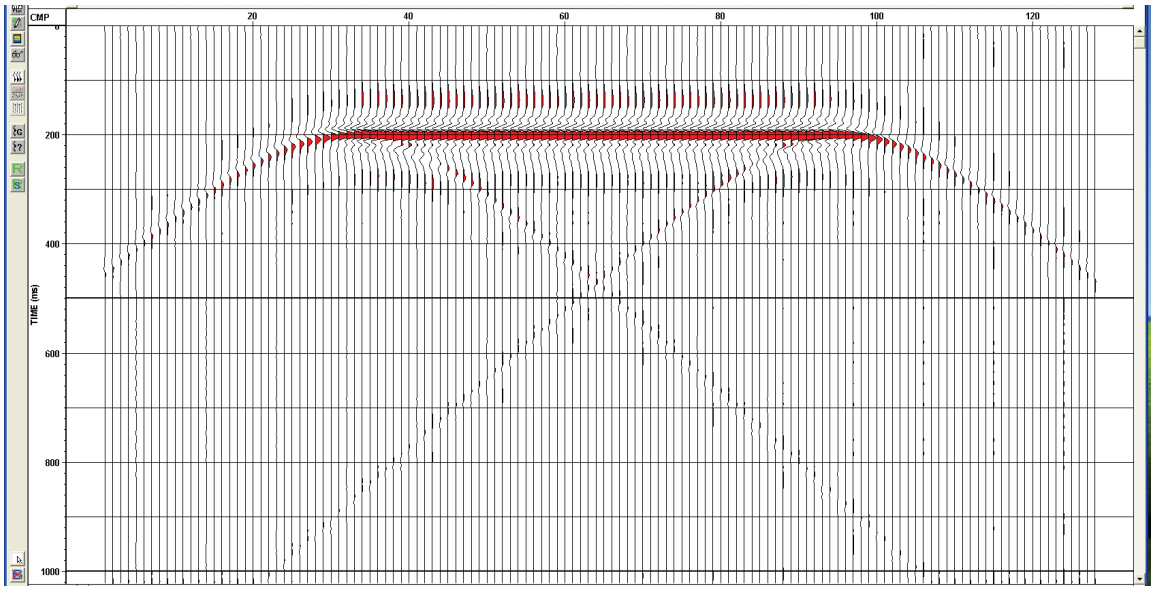

FIG. 9. A diffraction model produced with larger taper zones (5,15,50,75). The amplitude is 10 db above the amplitude at which the horizontal energy is one trace excursion.

Enlargements of Figure 9 are shown in Figure 10 with (a) showing a portion of the horizontal event and (b) a portion of the dipping event.

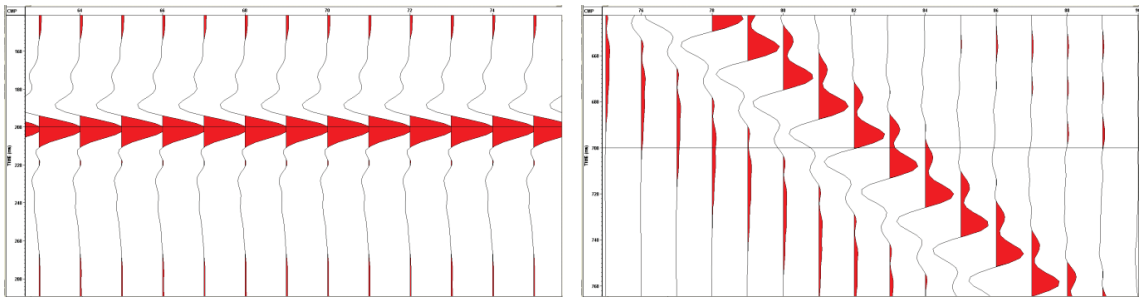

a) b)

FIG. 10. Expanded vies of the wavelet at a) the horizontal reflector, and b) a deeper part of the diffraction. The amplitude on this part of the diffraction was amplified by 30 db.

We can make a few more observation on the unaliased section regarding the phase of the wavelet. Notice the phase change of the wavelet in the center of the reflection of Figure 10a. The phase shift is 45 degrees. This coincides with the Rho filter or square-root derivative that is part of the theoretical development in 2D Kirchhoff migration. However, the wavelet in diffraction modelling is time reversed from the wavelet in

Kirchhoff migration, or equivalently, they have opposite phase. The phase of the wavelets will cancel if a section is created with diffraction modelling, then migrated with a Kirchhoff algorithm. However, both wavelets apply an amplitude attenuation proportional to the square root of the frequency, that will combine to produce an attenuation proportional to the frequency.

The wavelet on the steeper part of the diffraction was amplified, relative to the horizontal event by 30 db. It is displaying a wavelet with a 90 degree phase shift.

Diffraction amplitudes at the end of a reflection

Figure 11 compares the diffraction off the end or a reflector with a diffraction from a single point. The scatter point is 100 ms below the end of the reflection at CMP 100. It is plotted in this manner to compare the difference in the amplitudes of the simulated diffraction off the edge of a horizontal event with that of the diffraction which was used to model the reflection.

The amplitude of the diffraction was increased by a factor of three to match the peak amplitude of the wavelet at CMP 100. This amplitude is one-half that of the central portion of the horizontal reflector. Note the difference in the amplitudes of the "true" diffraction from the reflector and that of the point diffraction plotted below, even though the amplitudes match at the edge of the reflector.

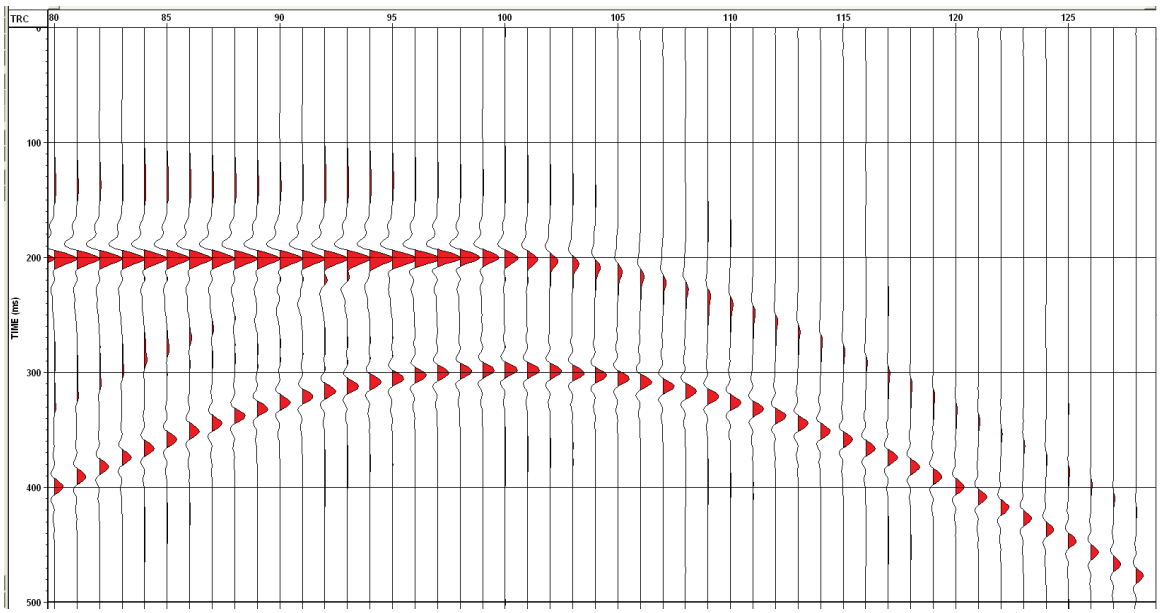

FIG. 11. Comparison of a diffraction off the end of a reflector with that of the diffraction used to create the reflection.

Earlier modelling techniques would simply add a diffraction to the end of the filtered horizontal event. The amplitude at the peak of the diffraction was half that of the horizontal reflector with a positive amplitude for CMPs beyond the end of the reflector, and negative amplitudes for CMPs below the reflector.

In order to compare the amplitudes of the diffraction over a greater interval, the single diffraction is placed at CMP 20 and the edge of the reflector starting at CMP 40. The four images in Figure 12 are the same data with different amplitude scales. The first image (a) has an amplitude scaled for the central peak to equal one trace interval, with the remaining plots (b) through (d) showing amplitude increases of 8, 16, and 24 db.

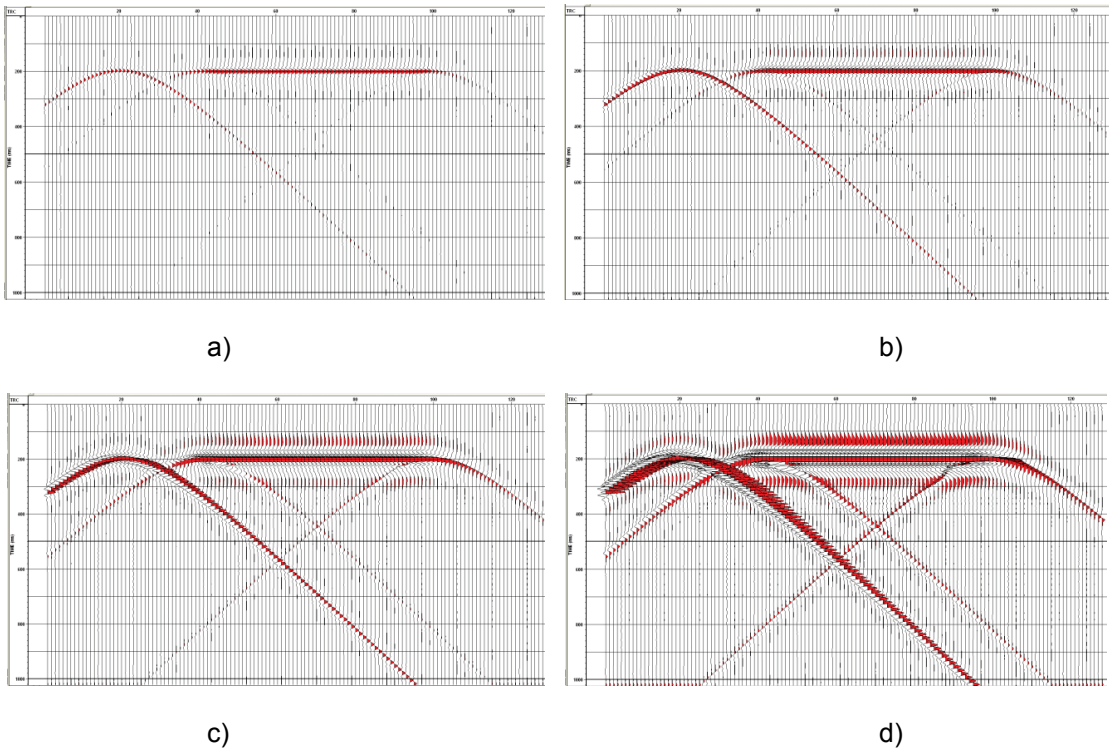

FIG. 12 A point diffraction placed at the same time but twenty traces to the left of the horizontal reflection at a) -24 db, b) -16 db, c) at -8 db, and d) at 0 db.

Once again we can see the attenuation of the edge diffraction is more rapid than that of the point diffraction. The apex of the diffraction is at t_0 = 200 ms. The amplitude difference at time t = 400 ms is approximately 12 db or a factor of four. The modelling diffraction has an amplitude attenuation of t_0/t, giving the reflector diffraction an amplitude of $(t_0/t)^3$ at this time, though the actual amplitude function will be much more complex.

The migration of terminated reflectors and scatterpoints

The difference of the diffractions on a terminated reflector with a scatterpoint diffraction does have an impact on tests created to evaluate migrations. In some of these tests, many scatterpoints are created at various locations in the reflectivity section then modelled to produce diffractions. These diffractions are then migrated to evaluate the quality of the migration including the effects of truncating the diffractions in space and time. These tests indicate that adequate focusing of the scatterpoint energy requires large migration apertures and high dip angles. While these tests are valid for scatterpoints,

they may not provide similar information about the focusing of a terminated event, such as one truncated by a fault. Because of the reduced amplitudes in the diffraction of the truncated event, adequate focusing may be accomplished with a smaller dip limit and offsets than anticipated when focusing a scatterpoint.

A Kirchhoff migration was applied to the above data with dip limits tapered from 85 to 90 degrees. The input data has a lagging wavelet due to its construction using diffractions. Kirchhoff migration (without the Rho filter) produces a leading wavelet that removes the modelling phase shift as illustrated by the migration result in Figure 13a. The wavelet is now zero phase.

Note the very sharp edge of the migrated horizontal event at CMP 40.

The Kirchhoff algorithm used in these tests had the capability of applying various methods for antialias filtering (AAF). Figure 13b included an antialiasing triangle filter in the migration, and its effect can be visualized by the edge at CMP 40 where there is some spatial smearing of the data.

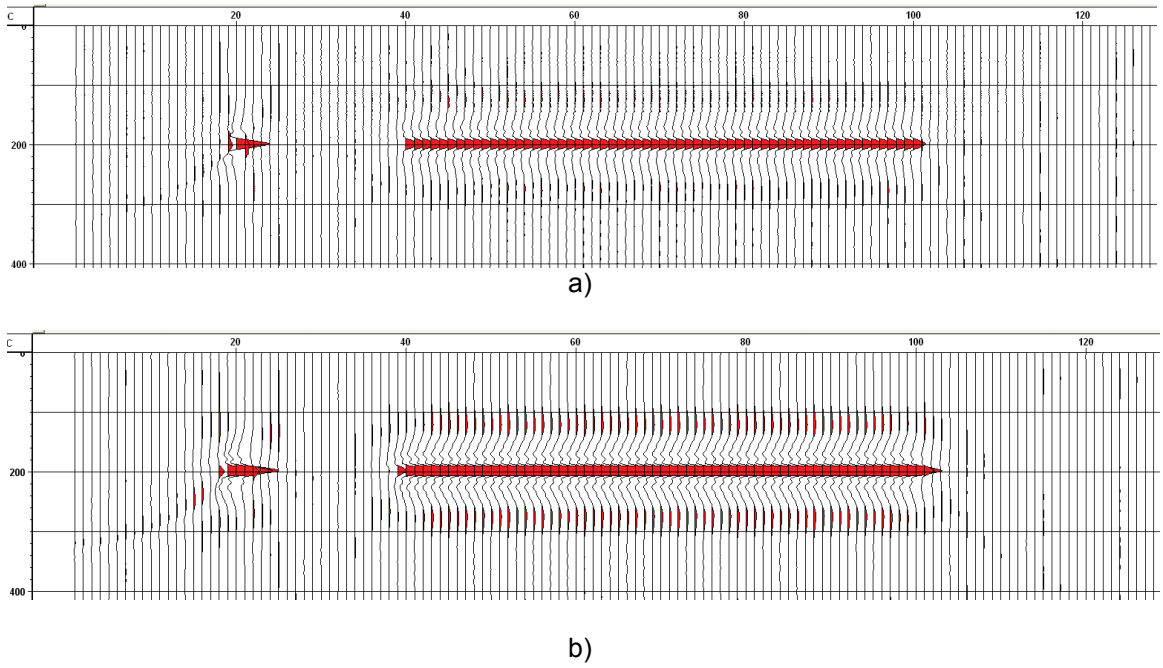

FIG. 13 A Kirchhoff migration of the previous model using a) no AAF and b) a triangle filter AAF.

Dip limited migrations

The following images show zoomed images for various dip limited Kirchhoff migrations of the modelled data in Figure 11. Data on the left was migrated without an AAF while the data on the right was migrated using an AAF. Dip limits of 85-89, 45-60, and 30-35 degrees were applied.

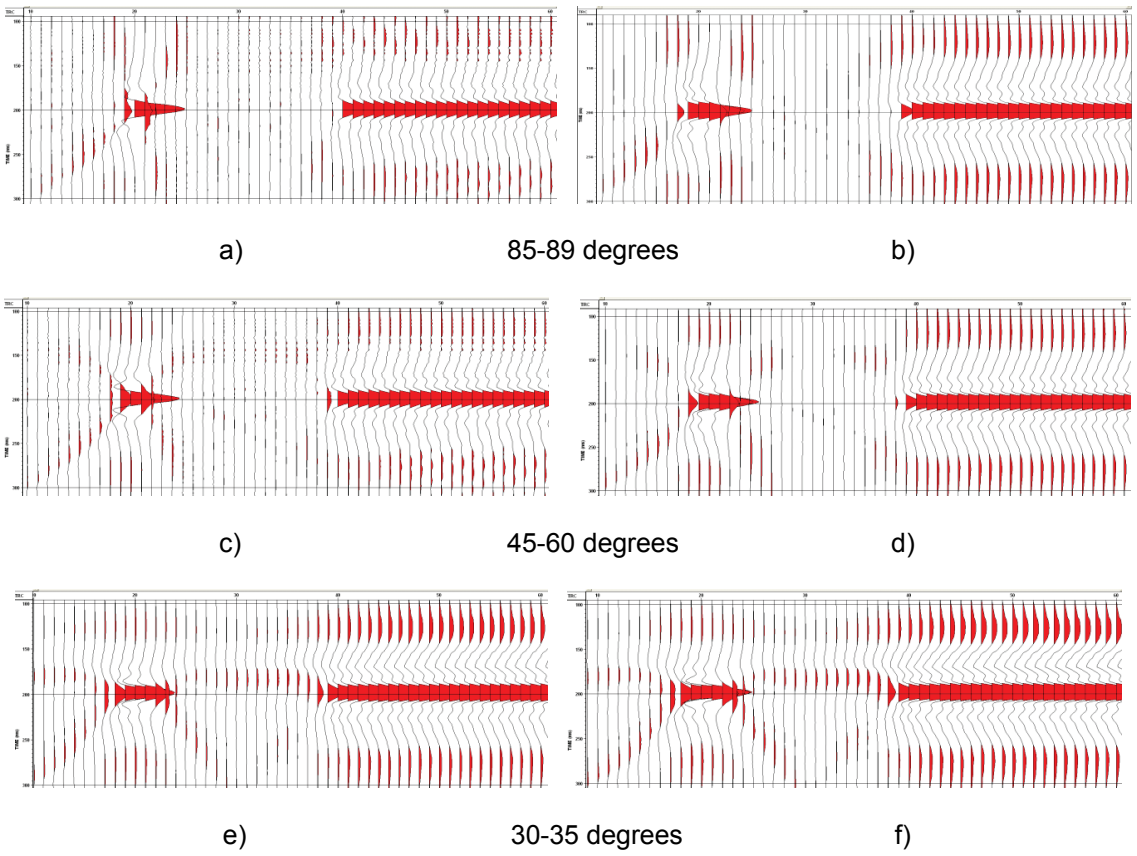

FIG. 14 Zoomed views of a point and modelled with diffractions and Kirchhoff migrated. The left side used no AAF while the right side used a triangle filter AAF. Each row used the indicated migration dip limit. The peak amplitude of the horizontal event is approximately two trace intervals.

Note that the lateral smearing of energy from the scatterpoint is greater than that from the terminated reflector.

COMMENTS AND CONCLUSIONS

The modelling of seismic data was accomplished by substituting diffractions on a time section that correspond to scatterpoint locations. We may refer to this process as spreading the energy along a diffraction, and in a constant velocity environment this is identical to summing energy on a semicircle. The effect of modelling data with a single time sample on the diffraction was used to illustrate aliasing and methods used to reduce its effect.

The difference in a diffraction from a truncated event and that from a scatterpoint were displayed and discussed. The amplitudes along a truncated diffraction attenuate much faster, and may allow less stringent constraints on the migration algorithm, than those from scatterpoints.

An aliased operator can produce aliased events on input data, even on horizontal events that are often assumed to be free from aliasing.

Migration is similar to modelling, but in a constant velocity environment, the migration operator spreads energy along a semicircle. Migration may also sum energy along a diffraction and is referred to as Kirchhoff migration. The same aliasing effects of diffraction modelling apply to Kirchhoff migration in that an aliased operator can produce aliased events above a horizontal reflector. Antialiasing filters are, or should be used with Kirchhoff migration. The same type of AAF filter should be used when modelling with diffractions, where the wavelet varies with offset. As the offset increases along the diffraction, the dip also increases and the frequency of the required high cut filter should be determined using equation (2).

The migration in Figure 15 has been included to illustrate the problem of aliasing in a Kirchhoff migration. An AAF was only applied to the right-hand side of the data. Note the aliased noise from the dipping events on the left, but more relevant to this paper, note the aliased horizontal events above horizontal reflector.

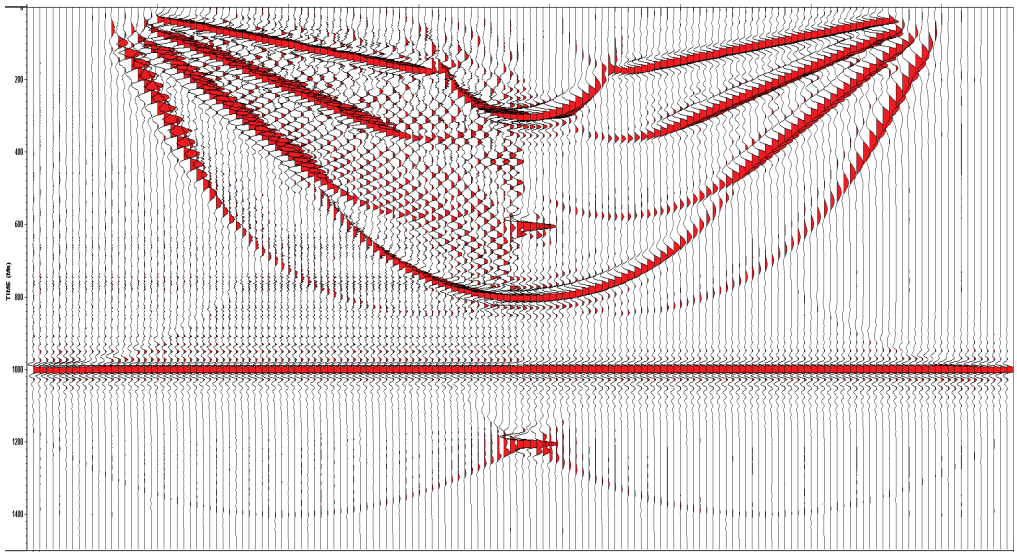

FIG. 15 An example of a Kirchhoff migration on a simple constant velocity section to illustrate operator aliasing. An AAF was only applied to the right hand side of the data.

Modelling and Kirchhoff migration produce similar wavelet distortions but with opposite phase. The wavelet distortion may be corrected using a Rho filter which, for migration, is a square-root derivative. Diffraction modelling followed by a Kirchhoff migration with no Rho filter correction will produce a zero phase wavelet as the phase distortions will cancel. However the amplitude spectrum of the wavelet will be different and will be the product of the amplitude spectrums of the Rho filters.

A considerable investment has been expended in developing antialiasing filters for Kirchhoff migration. These filters could be computed for each point on all diffractions. However, a library of these filters could be created and ordered by dip. Other filters could be extracted from a single high resolution filter. However, I have found the "triangle filter" to be very efficient, and it adds little runtime to the migration process.

I have seen many examples where AAFs have not used when using Kirchhoff migration. The objective of not using the AAFs was to reduce the computational times of the migration. The resulting migrations have often been branded inferior to other migration algorithms because of the presence of aliased energy.

Modelling with diffractions could benefit from migration by using the same AAFs. The triangle filter comes highly recommended.

ACKNOWLEDGEMENTS

I am grateful for the financial support of the CREWES sponsors.

SOFTWARE

The software for the examples used in this paper came from laboratory exercises written for a modelling and migration course. The displays were created using the VISTA seismic processing package.

REFERENCES

No references are included in this report. However, all the related material may be found in my course notes “A Practical Understanding of Poststack Migration” and “A Practical Understanding of Prestack Migration”.